Near-infrared emission in Ho^{3+}-doped $Yb_3Ga_5O_{12}$ garnet nanocrystals

T. Netolicky[1*], L. Benes[2], K. Melanova[2], S. Slang[3], J. Oswald[4], T. Wagner[1,3]

[1]*Department of General and Inorganic Chemistry, Faculty of Chemical Technology, University of Pardubice, Studentska 573, 53210 Pardubice, Czech Republic*

[2]*Joint Laboratory of Solid State Chemistry, Faculty of Chemical Technology, University of Pardubice, Studentska 95, 53210 Pardubice, Czech Republic*

[3]*Center of Materials and Nanotechnologies, Faculty of Chemical Technology, University of Pardubice, Cs. Legii 565, 530 02 Pardubice, Czech Republic*

[4]*Institute of Physics of the Czech Academy of Sciences, Cukrovarnicka 10, 162 00 Prague 6, Czech Republic*

[*]*Tomas Netolicky E-mail: tomas.netolicky2@student.upce.cz*

Abstract

The single-phase Ho^{3+}-doped $Yb_3Ga_5O_{12}$ garnet nanocrystals were synthesized by the sol-gel combustion technique using citric acid. Their structure, morphology and chemical composition were examined by the powder X-ray diffraction and Energy-dispersive X-ray spectrometry with the scanning electron microscope. The observed strong absorption band associated with the high content of Yb^{3+} ensures efficient excitation of the $Yb_{15-x}Ho_xGa_{25}O_{60}$ garnets using 980 nm radiation. The near-infrared emission originating from the Ho^{3+}: $^5I_6 \rightarrow {}^5I_8$ and $^5I_7 \rightarrow {}^5I_8$ transitions is studied using the measurement of the steady-state and time-dependent emission spectra. The proposed luminescence mechanism is discussed based on the $Yb^{3+} \rightarrow Ho^{3+}$ energy transfer with contribution of the $Ho^{3+} \rightarrow Yb^{3+}$ energy back transfer and $Ho^{3+} \leftrightarrow Ho^{3+}$ cross-relaxation processes.

Keywords: $Yb_3Ga_5O_{12}$ garnet; Ho^{3+}-doped garnet; near-infrared emission; lifetime; sol-gel combustion

1. Introduction

Among the rare-earth (RE^{3+}) ions, Ho^{3+} is one of the great interest luminescent activator in the near-infrared region owing to $^5I_6 \rightarrow {}^5I_8$ and $^5I_7 \rightarrow {}^5I_8$ radiative transitions observed at wavelengths of ≈1.2 μm

and ≈2.0 μm, respectively [1–4]. The near-infrared emission possesses many features that make it attractive for various applications such as biological imaging [5], solid state lasing [6] or atmosphere pollution monitoring [7]. Unfortunately, direct excitation of Ho^{3+} ions by commercially available high-power InGaAs laser diode (980 nm) is inefficient due to the absence of a suitable absorption band. However, this problem can be solved by using suitable sensitizers: Er^{3+}, Tm^{3+} and/or Yb^{3+} [8–10]. Compared with Er^{3+} and Tm^{3+}, Yb^{3+} is more feasible considering broad absorption band, large absorption cross section at 980 nm and presence of only one excited level $^2F_{5/2}$ [11]. Thus, the excitation of the Ho^{3+}-Yb^{3+} pair by 980 nm laser diode leads firstly to population of the Yb^{3+}: $^2F_{5/2}$ energy level and the absorbed energy is subsequently transferred to the neighbouring Ho^{3+} ions.

Host lattice is another circumstance which can significantly affect the luminescence dynamics. Low maximum phonon energy as well as low hydroxyl-group content of the doped host material are preferred for reduction of non-radiative processes [12, 13]. Generally, oxide garnets show relatively low maximum phonon energies [14, 15] with excellent mechanical, thermal and chemical properties in both monocrystalline [16, 17] and polycrystalline form [18, 19]. Ytterbium gallium garnet ($Yb_3Ga_5O_{12}$) belongs to the cubic crystalline system, with the space group $Ia\bar{3}d$ [20]. $Yb_3Ga_5O_{12}$ with excellent predicted phase stability [21] and high Yb^{3+} content can be utilized as a promising host for Ho^{3+} ions. So far, although the upconversion photoluminescence in oxide micro/nanophosphors containing Ho^{3+} and Yb^{3+} ions has been reported [22–24], the works about ≈1.2 μm and ≈2.0 μm emissions have been rarely reported [25].

In this work, we synthesized for the first time the Ho^{3+}-doped $Yb_3Ga_5O_{12}$ nanocrystalline powders via the sol-gel combustion technique. Luminescence spectra in the near-infrared region were studied under 980 nm excitation as well as appropriate luminescence lifetimes. Furthermore, energy transfer mechanism between Yb^{3+} and Ho^{3+} was discussed systematically.

2. Experimental details

The garnet nanocrystals of composition $Yb_{15-x}Ho_xGa_{25}O_{60}$ with x = 0.01, 0.1, 0.5, 1 and 2 at.% were synthesized by a sol-gel combustion technique. High purity Ga (5N, HiChem) together with Yb_2O_3 and Ho_2O_3 (both 3N, HiChem) were dissolved in high-purity nitric acid. The excess HNO_3 was removed at high temperature. The metal nitrates dissolved in deionized water were subsequently chelated by citric acid (molar ratio of citric acid:total metal ions = 2.5:1). The pH of the stirred solution was set to pH ≈8 (at ≈25 °C) by dropwise addition of highly-pure ammonia solution. The solution was heated to ≈90 °C under rigorous stirring to form a homogenous transparent-to-pink gel. The dried gel was decomposed in a furnace at 800 °C for 2 h and subsequently at 1000 °C for ½ h to form white powder. Details of the synthetic procedure can be found in the previous work [26].

The crystalline structure of the prepared samples was examined by X-ray diffractometer Bruker D8 ADVANCE in the Bragg-Brentano geometry equipped with Cu $K\alpha$ radiation (λ = 1.5406 Å). The scanning range and step of the 2θ angle were 5–90° and ≈0.009°, respectively. The X-ray diffraction (XRD) patterns were analyzed with the use of EVA software (EVA, ver.19, Diffracplus Basic Evaluating Package; Bruker AXS GmbH, 2013). The chemical composition of the prepared samples was studied by Energy-dispersive X-ray (EDX) spectrometer AZtec X-Max 20 (Oxford Instruments) attached to LYRA 3 scanning electron microscope (SEM, TESCAN). The chemical composition (measured at U = 20 kV) was determined as an average value from 5 measured points of each sample. The same device was used for SEM scans acquisition. Diffuse reflectance spectra were recorded in the wavelength range of 200–1800 nm by a UV-Vis-NIR spectrophotometer JASCO V-570, and the scanning step was 1 nm. For the photoluminescence (PL) measurements, the excitation radiation of a wavelength of 980 nm emitted by a cw laser POL 4300 was used and the light was processed by a double grated SDL-1 monochromator. Steady-state emission spectra were recorded in the spectral region of 1050–1350 nm for the Ho^{3+}: $^5I_6 \rightarrow {}^5I_8$ transition and in the spectral region of 1800–2300 nm for the Ho^{3+}: $^5I_7 \rightarrow {}^5I_8$ transition. The scanning step was between 0.5 and 1 nm. Luminescence signal was detected by a thermoelectrically cooled InGaAs detector. The decay curves of the Ho^{3+}: $^5I_6 \rightarrow {}^5I_8$ and $^5I_7 \rightarrow {}^5I_8$ transitions were recorded using a digital oscilloscope with a pulse width of ≈30 μs. The Ho^{3+} decay curves were evaluated by single exponential function. All measurements were carried out at room temperature.

3. Results and discussion

3.1. Structural properties

Fig. 1 shows the XRD patterns of prepared $Yb_{15-x}Ho_xGa_{25}O_{60}$ (x = 0.01, 0.1, 0.5, 1 and 2 at.%) nanocrystalline samples. The XRD patterns of the samples confirm formation of single-phase cubic $Yb_3Ga_5O_{12}$ garnets (space group $Ia\bar{3}d$). Table 1 presents average crystallite size and lattice parameter of the samples. The average crystallite size was determined by Scherrer equation [27] and the values range from ≈27 to ≈34 nm.

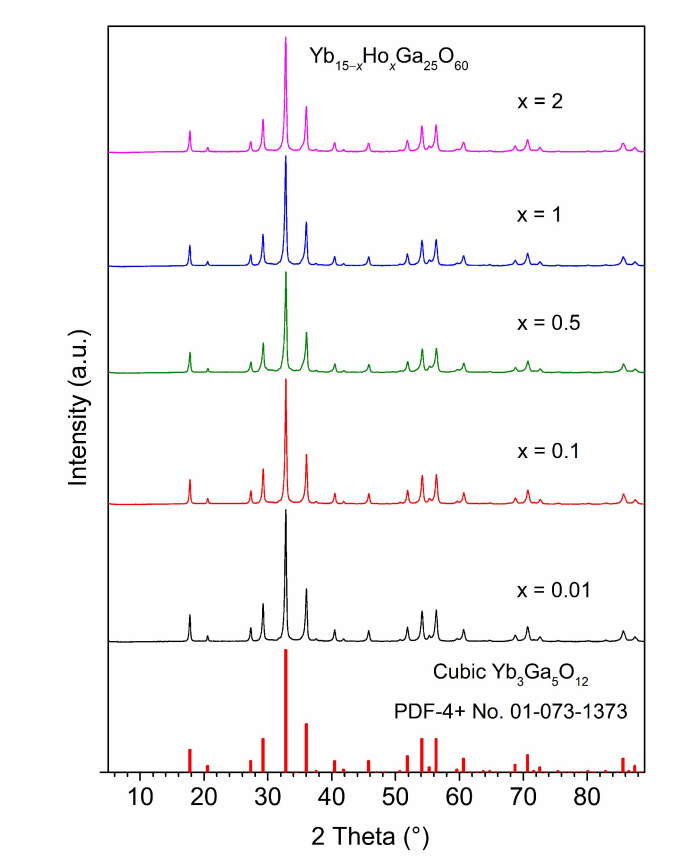

Fig. 1. Powder XRD patterns of prepared $Yb_{15-x}Ho_xGa_{25}O_{60}$ nanocrystals.

Table 1 Average crystallite size (*d*) and lattice parameter (*a*) of prepared $Yb_{15-x}Ho_xGa_{25}O_{60}$ nanocrystals.

x (at.%)	*d* (nm)	*a* (Å)
0.01	32.5	12.2052
0.1	34.3	12.1994
0.5	27.3	12.1968
1	30.1	12.2072
2	29.5	12.2085

3.2. Morphology and chemical composition

Fig. 2 presents typical image from SEM of $Yb_{14.9}Ho_{0.1}Ga_{25}O_{60}$ sample. Highly porous sample is formed by many agglomerates which is a typical feature for nanocrystals prepared by sol-gel combustion technique using citric acid [26, 28]. Chemical composition of five $Yb_{15-x}Ho_xGa_{25}O_{60}$ (x = 0.01, 0.1, 0.5, 1 and 2 at.%) nanocrystalline samples determined by EDX spectrometry is listed in Table 2. Theoretical composition is listed for comparison. Holmium was not detected in the $Yb_{14.99}Ho_{0.01}Ga_{25}O_{60}$ and $Yb_{14.9}Ho_{0.1}Ga_{25}O_{60}$ samples due to its low content. All of the samples show good conformity of the intended and determined chemical composition with respect to their character and measurement error.

Fig. 2. SEM image of $Yb_{14.9}Ho_{0.1}Ga_{25}O_{60}$ nanocrystalline sample. The scale is 1000 nm.

Table 2 Theoretical and EDX-determined chemical composition of prepared $Yb_{15-x}Ho_xGa_{25}O_{60}$ nanocrystals.

x (at.%)		Yb (at.%)	Ho (at.%)	Ga (at.%)	O (at.%)
0.01	Theoretical	14.99	0.01	25	60
	EDX	15.8	–	24.6	59.6
0.1	Theoretical	14.9	0.1	25	60
	EDX	16.7	–	25.7	57.6
0.5	Theoretical	14.5	0.5	25	60
	EDX	16.6	0.6	24.4	58.4
1	Theoretical	14.0	1.0	25	60
	EDX	14.2	1.0	24.3	60.5
2	Theoretical	13.0	2.0	25	60
	EDX	13.3	2.0	24.6	60.1

3.3. Diffuse reflectance properties

Diffuse reflectance spectra of prepared $Yb_{15-x}Ho_xGa_{25}O_{60}$ ($x = 0.01$, 0.1, 0.5, 1 and 2 at.%) nanocrystalline samples are shown in Fig. 3. The broad and strong absorption band with maximum at ≈925 nm corresponds to absorption by the Yb^{3+} ions from the $^2F_{7/2}$ ground state to the $^2F_{5/2}$ excited state level. Absorption bands centered at ≈1130, ≈640, ≈535, ≈485, ≈450, ≈415 and ≈365 nm may be attributed to the transitions of the Ho^{3+} from the $^5I_8$ ground state to the excited states $^5I_6$, $^5F_5$, $^5F_4/^5S_2$, $^5F_3/^5F_2/^3K_8$, $^5F_1/^5G_6$, $^5G_5$ and $^3H_6/^3H_5$, respectively. The $Yb_{15-x}Ho_xGa_{25}O_{60}$ garnets show fundamental absorption bellow 300 nm as well as was observed in the $Yb_{15-y}Er_yGa_{25}O_{60}$ garnets with *y*: 0–2 at.% [26]. Such a broad and

strong absorption band situated between ≈850 and ≈1050 nm is associated with high Yb^{3+} content in the studied $Yb_{15-x}Ho_xGa_{25}O_{60}$ garnets and makes these garnets suitable for efficient pumping by InGaAs laser.

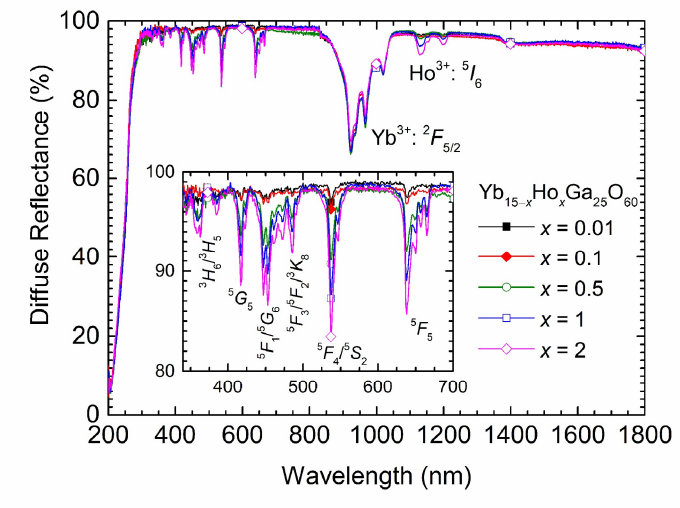

Fig. 3. Diffuse reflectance spectra of $Yb_{15-x}Ho_xGa_{25}O_{60}$ nanocrystals. Inset shows detail of diffuse reflectance spectra in the 350–700 nm region.

3.4. Luminescence properties

The Ho^{3+}: $^5I_6 \rightarrow {}^5I_8$ emission spectra of $Yb_{15-x}Ho_xGa_{25}O_{60}$ (x = 0.01, 0.1, 0.5, 1 and 2 at.%) nanocrystalline samples under 980 nm excitation are shown in Fig. 4. The variation of integrated PL intensity with x from the inset of Fig. 4 shows non-linear increment from x = 0.01 to x = 1. The observed decrease of integrated PL intensity of $Yb_{13}Ho_2Ga_{25}O_{60}$ sample is assigned to concentration quenching effect [29]. Nevertheless, the integrated PL intensity of $Yb_{13}Ho_2Ga_{25}O_{60}$ sample is still relatively high and comparable to that of $Yb_{14.5}Ho_{0.5}Ga_{25}O_{60}$ sample. Fig. 5 presents the Ho^{3+}: $^5I_7 \rightarrow {}^5I_8$ emission spectra of the $Yb_{15-x}Ho_xGa_{25}O_{60}$ nanocrystalline garnets. The integrated PL intensity from the inset of Fig. 5 shows maximum here for x = 0.5 and significant decrease of integrated PL intensity is observed for x > 0.5. This suggests that population and depopulation of the $^5I_6$ and $^5I_7$ energy levels include different mechanisms.

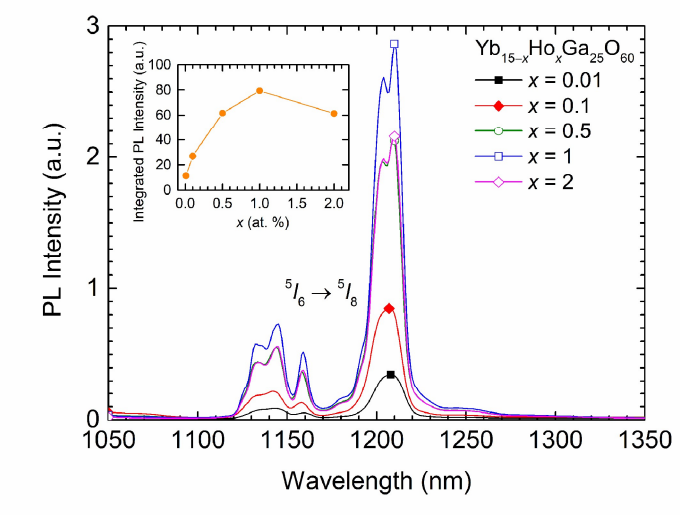

Fig. 4. Emission spectra of $Yb_{15-x}Ho_xGa_{25}O_{60}$ nanocrystals from 1050 to 1350 nm under excitation wavelength of 980 nm with excitation intensity of 10 W/cm^2. Inset shows the variation of integrated PL intensity with x. The line from inset serves as a guide for the eye.

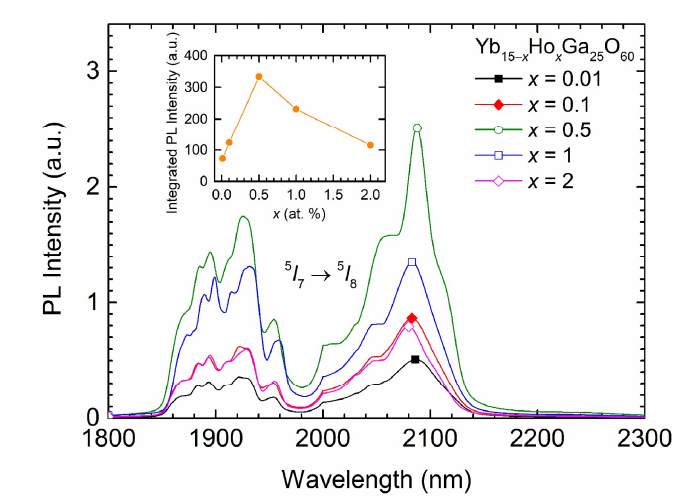

Fig. 5. Emission spectra of $Yb_{15-x}Ho_xGa_{25}O_{60}$ nanocrystals from 1800 to 2300 nm under excitation wavelength of 980 nm with excitation intensity of 10 W/cm^2. Inset shows the variation of integrated PL intensity with x. The line from inset serves as a guide for the eye.

To further clarify the different origin of the Ho^{3+}: $^5I_6 \rightarrow {}^5I_8$ and $^5I_7 \rightarrow {}^5I_8$ radiative transitions in the $Yb_{15-x}Ho_xGa_{25}O_{60}$ nanocrystalline garnets, the decay curves were recorded at the strongest emission wavelengths. The Ho^{3+}: $^5I_6 \rightarrow {}^5I_8$ emission decay curves were measured at 1209 nm and are presented in Fig. 6. The emission decay curves for the Ho^{3+}: $^5I_7 \rightarrow {}^5I_8$ transition were measured at 2087 nm and are shown in Fig. 7. Both the Ho^{3+}: $^5I_6 \rightarrow {}^5I_8$ and $^5I_7 \rightarrow {}^5I_8$ radiative transitions exhibit a single exponential decaying behaviour. The respective lifetime values $\tau(^5I_6 \rightarrow {}^5I_8)$ and $\tau(^5I_7 \rightarrow {}^5I_8)$ were obtained by fitting the data by the function: $y = y_0 + A_1 \cdot \exp(-x/\tau)$, where y_0 and A_1 are the off-set and pre-factor, respectively.

The lifetimes $\tau(^5I_6 \rightarrow {}^5I_8)$ and $\tau(^5I_7 \rightarrow {}^5I_8)$ are listed in Table 3 and graphically illustrated in the insets of Figs. 6 and 7 for respective x in the $Yb_{15-x}Ho_xGa_{25}O_{60}$ nanocrystals. The lifetime $\tau(^5I_6 \rightarrow {}^5I_8)$ exhibits slight increase with increasing x from ≈245 μs (x = 0.01) to ≈272 μs (x = 2) suggesting population of the $^5I_6$ level by cross-relaxation (CR) processes [8, 30, 31]. The lifetime $\tau(^5I_7 \rightarrow {}^5I_8)$ exhibits higher sensitivity to x in the $Yb_{15-x}Ho_xGa_{25}O_{60}$ nanocrystals when compared with the $\tau(^5I_6 \rightarrow {}^5I_8)$. The $\tau(^5I_7 \rightarrow {}^5I_8)$ first increases from ≈15.63 ms (x = 0.01) to ≈16.38 ms (x = 0.1) and subsequently a significant decrease occurs for $x > 0.1$ up to ≈2.02 ms (x = 2). The observed $\tau(^5I_7 \rightarrow {}^5I_8)$ decrease for $x > 0.1$ in the $Yb_{15-x}Ho_xGa_{25}O_{60}$ nanocrystals suggests efficient depopulation of the $^5I_7$ level by CR processes and concentration quenching effect [8, 29–31].

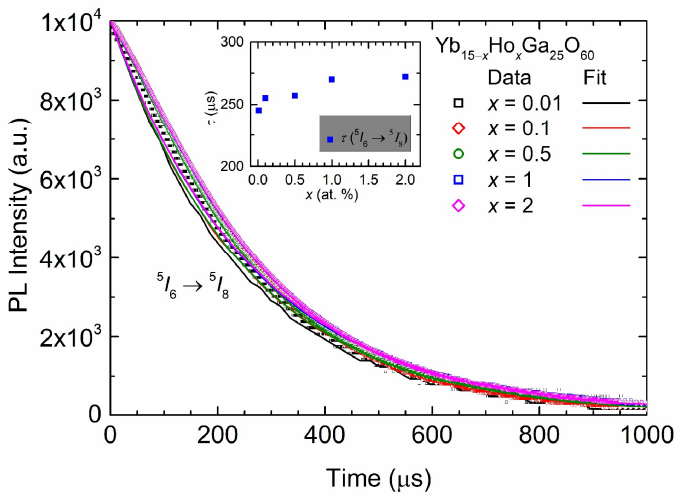

Fig. 6. Normalised decay curves of the Ho^{3+}: $^5I_6 \rightarrow {}^5I_8$ emission in $Yb_{15-x}Ho_xGa_{25}O_{60}$ nanocrystals under excitation wavelength of 980 nm with excitation intensity of 12 W/cm^2. Inset shows the variation of $\tau(^5I_6 \rightarrow {}^5I_8)$ with x.

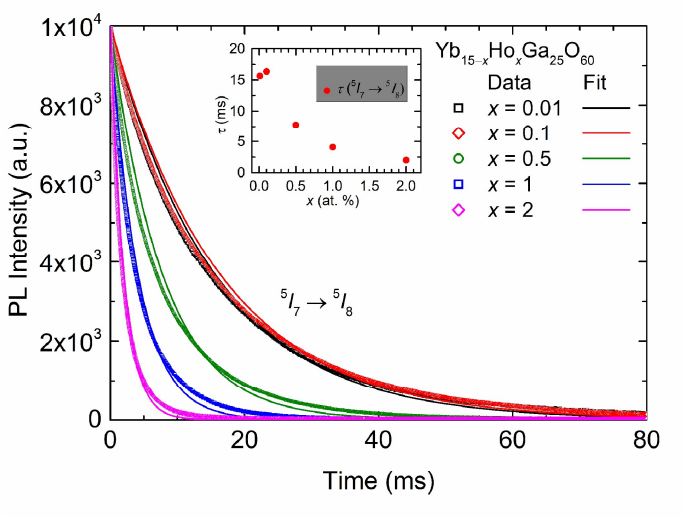

Fig. 7. Normalised decay curves of the Ho^{3+}: $^5I_7 \rightarrow {}^5I_8$ emission in $Yb_{15-x}Ho_xGa_{25}O_{60}$ nanocrystals under excitation wavelength of 980 nm with excitation intensity of 12 W/cm^2. Inset shows the variation of $\tau(^5I_7 \rightarrow {}^5I_8)$ with x.

Table 3 Lifetime values of the Ho^{3+}: $^5I_6 \rightarrow {}^5I_8$ and $^5I_7 \rightarrow {}^5I_8$ emission in $Yb_{15-x}Ho_xGa_{25}O_{60}$ nanocrystals.

x (at.%)	$\tau(^5I_6 \rightarrow {}^5I_8)$ (μs)	$\tau(^5I_7 \rightarrow {}^5I_8)$ (ms)
0.01	245±1	15.63±0.01
0.1	255±1	16.38±0.01
0.5	257±1	7.77±0.01
1	270±1	4.13±0.01
2	272±1	2.02±0.01

In order to explain the near-infrared emission mechanism in the $Yb_{15-x}Ho_xGa_{25}O_{60}$ nanocrystalline garnets, Fig. 8 presents the energy level diagram of Ho^{3+} and Yb^{3+} ions. When the garnets are excited by 980 nm wavelength laser, firstly the Yb^{3+} ions in the $^2F_{7/2}$ ground state are pumped to the $^2F_{5/2}$ excited state. The absorbed energy is then transferred to the neighbouring Ho^{3+} ions by energy transfer process ET1: $^2F_{5/2}$ (Yb^{3+}) + $^5I_8$ (Ho^{3+}) → $^2F_{7/2}$ (Yb^{3+}) + $^5I_6$ (Ho^{3+}), which populates the $^5I_6$ level of the Ho^{3+}. Subsequently, three different processes can take place from the Ho^{3+}: $^5I_6$ level. (1) The radiative transition to the ground state of the Ho^{3+} ($^5I_6 \rightarrow {}^5I_8$) providing the observed ≈1.2 μm emission. (2) The nonradiative relaxation (NR) to the lower-lying $^5I_7$ level. (3) The energy transfer process ET2: $^2F_{5/2}$ (Yb^{3+}) + $^5I_6$ (Ho^{3+}) → $^2F_{7/2}$ (Yb^{3+}) + $^5F_4/^5S_2$ (Ho^{3+}) in combination with the excited state absorption process ESA1: $^5I_6$ (Ho^{3+}) + a photon → $^5F_4/^5S_2$ (Ho^{3+}). Since the process (2) populates the Ho^{3+}: $^5I_7$ level, the observed ≈2 μm emission is provided by the radiative transition to the ground state of the Ho^{3+} ($^5I_7 \rightarrow {}^5I_8$). Part of the energy from the Ho^{3+}: $^5I_7$ level can populate the Ho^{3+}: $^5F_5$ level by energy transfer process ET3: $^2F_{5/2}$ (Yb^{3+}) + $^5I_7$ (Ho^{3+}) → $^2F_{7/2}$ (Yb^{3+}) + $^5F_5$ (Ho^{3+}) in combination with the excited state absorption process ESA2: $^5I_7$ (Ho^{3+}) +

a photon → $^5F_5$ (Ho^{3+}). The Ho^{3+}: $^5F_4/^5S_2$ levels pumped by process (3) may be efficiently depleted by NR to the lower-lying $^5F_5$ level in combination with energy back transfer (EBT) process. Since the EBT process: $^5F_4/^5S_2$ (Ho^{3+}) + $^2F_{7/2}$ (Yb^{3+}) → $^5I_6$ (Ho^{3+}) + $^2F_{5/2}$ (Yb^{3+}) has been proved in materials with high Yb^{3+}/Ho^{3+} content [30, 32, 33], it is inevitably present in the studied $Yb_{15-x}Ho_xGa_{25}O_{60}$ garnets. Furthermore, CR processes can take place between two Ho^{3+} ions, i.e. CR1: $^5F_4/^5S_2 + {}^5I_7 \rightarrow {}^5F_5 + {}^5I_6$ and CR2: $^5I_7 + {}^5I_7 \rightarrow {}^5I_8 + {}^5I_6$ [8, 30, 31]. The probability of the CR1 and CR2 processes increases with increasing x in the $Yb_{15-x}Ho_xGa_{25}O_{60}$ garnets leading to depopulation of the Ho^{3+}: $^5I_7$ level which can explain the observed $\tau(^5I_7 \rightarrow {}^5I_8)$ decrease for $x > 0.1$. The observed non-decreasing $\tau(^5I_6 \rightarrow {}^5I_8)$ even for the $Yb_{13}Ho_2Ga_{25}O_{60}$ sample suggests efficient ET1 process with contribution of the CR1, CR2 and EBT processes.

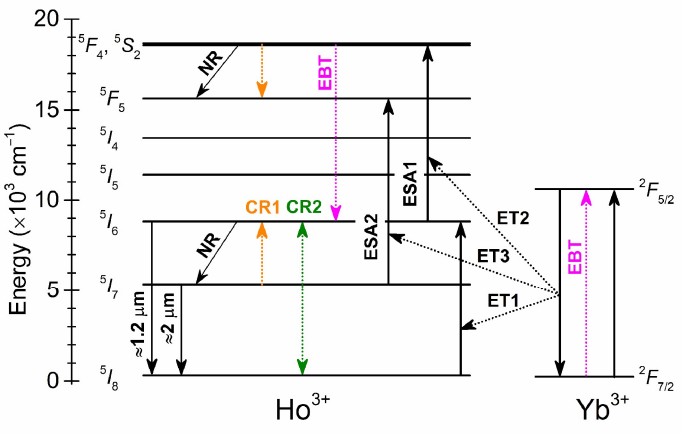

Fig. 8. Schematic energy level diagram of Ho^{3+} and Yb^{3+} ions in the Ho^{3+}-doped $Yb_3Ga_5O_{12}$ with proposed near-infrared emission mechanism under excitation wavelength of 980 nm.

4. Conclusions

The single-phase Ho^{3+}-doped $Yb_3Ga_5O_{12}$ nanocrystals with 0.01, 0.1, 0.5, 1 and 2 at.% Ho^{3+} were synthesized by the sol-gel combustion technique using citric acid. Phase composition, morphology and chemical composition were verified by XRD and EDX-SEM analysis. All prepared nanocrystals exhibit high optical reflectivity in visible and near-infrared region with strong and broad absorption band observed from ≈850 to ≈1050 nm due to the Yb^{3+}: $^2F_{7/2} \rightarrow {}^2F_{5/2}$ transition. Excited by 980 nm, two radiative transitions of the Ho^{3+}: $^5I_6 \rightarrow {}^5I_8$ and $^5I_7 \rightarrow {}^5I_8$ were observed in the wavelength regions of 1050–1350 nm and 1800–2300 nm, respectively. The lifetime $\tau(^5I_6 \rightarrow {}^5I_8)$ is very slightly increased with higher Ho^{3+} content. In contrast, the lifetime $\tau(^5I_7 \rightarrow {}^5I_8)$ is highly sensitive to Ho^{3+} content with maximum of ≈16.38 ms in the $Yb_{14.9}Ho_{0.1}Ga_{25}O_{60}$ sample and with further decrease for higher Ho^{3+} concentrations. Based on the energy level diagram describing energy transfer from Yb^{3+} to Ho^{3+}, it is concluded that the CR processes are responsible for quenching of the Ho^{3+}: $^5I_7$ level and these CR processes together with the EBT process

are responsible for pumping to the Ho^{3+}: $^5I_6$ level. The above results show that Ho^{3+}-doped $Yb_3Ga_5O_{12}$ nanocrystals are promising materials for the near-infrared emission.

Acknowledgements

The authors thank for financial support from the grant of the Ministry of Education, Youth and Sports of Czech Republic (grant LM2018103), the European Regional Development Fund Project, the project NANOMAT CZ.02.1.01/0.0/0.0/17_048/0007376 and the project of Faculty of Chemical Technology, University of Pardubice „Excellent teams“ 2020.

Declaration of Competing Interest

The authors declare that they have no known competing financial interests or personal relationships that could have appeared to influence the work reported in this paper.

References

[1] D. Dorosz, J. Zmojda, M. Kochanowicz, Investigation on broadband near-infrared emission in Yb^{3+}/Ho^{3+} co-doped antimony–silicate glass and optical fiber, Opt. Mater. 35 (2013) 2577–2580. https://doi.org/10.1016/j.optmat.2013.07.022.

[2] Y. Sun, Q. Yang, H. Wang, Y. Shao, Sensitization of Ho^{3+} on the 2.7 μm emission of Er^{3+} in $(Y_{0.9}La_{0.1})_2O_3$ transparent ceramics, J. Lumin. 194 (2018) 50–55. https://doi.org/10.1016/j.jlumin.2017.10.019.

[3] G. Hou, C. Zhang, W. Fu, G. Li, J. Xia, Y. Ping, Broadband mid-infrared 2.0 μm and 4.1 μm emission in Ho^{3+}/Yb^{3+} co-doped tellurite-germanate glasses, J. Lumin. 217 (2020) 116769. https://doi.org/10.1016/j.jlumin.2019.116769.

[4] P. Babu, I.R. Martín, V. Lavín, U.R. Rodríguez-Mendoza, H.J. Seo, K.V. Krishanaiah, V. Venkatramu, Quantum cutting and near-infrared emissions in Ho^{3+}/Yb^{3+} codoped transparent glass-ceramics, J. Lumin. 226 (2020) 117424. https://doi.org/10.1016/j.jlumin.2020.117424.

[5] E. Hemmer, N. Venkatachalam, H. Hyodo, A. Hattori, Y. Ebina, H. Kishimoto, K. Soga, Upconverting and NIR emitting rare earth based nanostructures for NIR-bioimaging, Nanoscale 5 (2013) 11339–11361. https://doi.org/10.1039/c3nr02286b.

[6] C. Zhao, Y. Hang, L. Zhang, J. Yin, P. Hu, E. Ma, Polarized spectroscopic properties of Ho^{3+}-doped $LuLiF_4$ single crystal for 2 μm and 2.9 μm lasers, Opt. Mater. 33 (2011) 1610–1615. https://doi.org/10.1016/j.optmat.2011.04.010.

[7] N. Sugimoto, N. Sims, K. Chan, D.K. Killinger, Eye-safe 2.1-μm Ho lidar for measuring atmospheric density profiles, Opt. Lett. 15 (1990) 302–304. https://doi.org/10.1364/OL.15.000302.

[8] R. Cao, Y. Lu, Y. Tian, F. Huang, Y. Guo, S. Xu, J. Zhang, 2 μm emission properties and nonresonant energy transfer of Er^{3+} and Ho^{3+} codoped silicate glasses, Sci. Rep. 6 (2016) 37873. https://doi.org/10.1038/srep37873.

[9] Z. Feng, S. Yang, H. Xia, C. Wang, D. Jiang, J. Zhang, X. Gu, Y. Zhang, B. Chen, H. Jiang, Energy transfer and 2.0 μm emission in Tm^{3+}/Ho^{3+} co-doped α-$NaYF_4$ single crystals, Mater. Res. Bull. 76 (2016) 279–283. https://doi.org/10.1016/j.materresbull.2015.11.063.

[10] B. Ding, X. Zhou, J. Zhang, H. Xia, H. Song, B. Chen, Ho^{3+} doped $Na_5Y_9F_{32}$ single crystals doubly sensitized by Er^{3+} and Yb^{3+} for efficient 2.0 μm emission, J. Lumin. 223 (2020) 117254. https://doi.org/10.1016/j.jlumin.2020.117254.

[11] J. Li, J. Zhang, Z. Hao, L. Chen, X. Zhang, Y. Luo, Intense Upconversion Luminescence of $CaSc_2O_4:Ho^{3+}/Yb^{3+}$ from Large Absorption Cross Section and Energy-Transfer Rate of Yb^{3+}, Chemphyschem 16 (2015) 1366–1369. https://doi.org/10.1002/cphc.201500011.

[12] H. Dong, G. Zhu, M. Zhang, K. Dai, Q. Li, C. Cui, Efficiently visible and 2 μm infrared emission in K_2YbF_5: Ce^{3+}/Ho^{3+} microcrystals, Curr. Appl. Phys. 20 (2020) 765–772. https://doi.org/10.1016/j.cap.2020.03.016.

[13] Y. Yan, A.J. Faber, H. de Waal, Luminescence quenching by OH groups in highly Er-doped phosphate glasses, J. Non-Cryst. Solids 181 (1995) 283–290. https://doi.org/10.1016/S0022-3093(94)00528-1.

[14] A. de Pablos-Martín, A. Durán, M.J. Pascual, Nanocrystallisation in oxyfluoride systems: mechanisms of crystallisation and photonic properties, Int. Mater. Rev. 57 (2012) 165–186. https://doi.org/10.1179/1743280411y.0000000004.

[15] Z. You, Y. Wang, J. Xu, Z. Zhu, J. Li, C. Tu, Diode-End-Pumped Midinfrared Multiwavelength Er:Pr:GGG Laser, IEEE Photon. Technol. Lett. 26 (2014) 667–670. https://doi.org/10.1109/LPT.2014.2302837.

[16] L. Mezeix, D.J. Green, Comparison of the Mechanical Properties of Single Crystal and Polycrystalline Yttrium Aluminum Garnet, Int. J. Appl. Ceram. Technol. 3 (2006) 166–176. https://doi.org/10.1111/j.1744-7402.2006.02068.x.

[17] C. Li, F. Zhang, B. Meng, X. Rao, Y. Zhou, Research of material removal and deformation mechanism for single crystal GGG ($Gd_3Ga_5O_{12}$) based on varied-depth nanoscratch testing, Mater. Des. 125 (2017) 180–188. https://doi.org/10.1016/j.matdes.2017.04.018.

[18] J. Li, Y. Wu, Y. Pan, W. Liu, L. Huang, J. Guo, Fabrication, microstructure and properties of highly transparent Nd:YAG laser ceramics, Opt. Mater. 31 (2008) 6–17. https://doi.org/10.1016/j.optmat.2007.12.014.

[19] E.E. Hellstrom, R.D. Ray II, C. Zhang, Preparation of Gadolinium Gallium Garnet [$Gd_3Ga_5O_{12}$] by Solid-State Reaction of the Oxides, J. Am. Ceram. Soc. 72 (1989) 1376–1381. https://doi.org/10.1111/j.1151-2916.1989.tb07656.x.

[20] G.A. Novak, G.V. Gibbs, The Crystal Chemistry of the Silicate Garnets, Am. Mineral. 56 (1971) 791–825.

[21] Z. Song, D. Zhou, Q. Liu, Tolerance factor and phase stability of the garnet structure, Acta Cryst. C75 (2019) 1353–1358. https://doi.org/10.1107/S2053229619011975.

[22] J.C. Boyer, F. Vetrone, J.A. Capobianco, A. Speghini, M. Bettinelli, Yb^{3+} ion as a sensitizer for the upconversion luminescence in nanocrystalline $Gd_3Ga_5O_{12}$:Ho^{3+}, Chem. Phys. Lett. 390 (2004) 403–407. https://doi.org/10.1016/j.cplett.2004.04.047.

[23] L. An, J. Zhang, M. Liu, S. Wang, Preparation and Upconversion Properties of Yb^{3+}, Ho^{3+}: Lu_2O_3 Nanocrystalline Powders, J. Am. Ceram. Soc. 88 (2005) 1010–1012. https://doi.org/10.1111/j.1551-2916.2005.00192.x.

[24] G. Gao, D. Busko, R. Joseph, A. Turshatov, I.A. Howard, B.S. Richards, High Quantum Yield Single-Band Green Upconversion in La_2O_3:Yb^{3+}, Ho^{3+} Microcrystals for Anticounterfeiting and Plastic Recycling, Part. Part. Syst. Charact. 36 (2019) 1800462. https://doi.org/10.1002/ppsc.201800462.

[25] G.H. Sun, Q.L. Zhang, J.Q. Luo, W.P. Liu, S. Han, L.L. Zheng, W.M. Li, Influence of Y^{3+} doping concentration on the structure and optical properties of Pr,Yb,Ho:GYTO polycrystalline powders, J. Lumin. 217 (2020) 116831. https://doi.org/10.1016/j.jlumin.2019.116831.

[26] T. Netolicky, L. Strizik, L. Benes, K. Melanova, S. Slang, T. Wagner, Deep red upconversion photoluminescence in Er^{3+}-doped $Yb_3Ga_5O_{12}$ nanocrystalline garnet, J. Am. Ceram. Soc. 105 (2022) 1–12. https://doi.org/10.1111/jace.18313.

[27] P. Scherrer, Bestimmung der Größe und der inneren Struktur von Kolloidteilchen mittels Röntgenstrahlen, Nachrichten von der Gesellschaft der Wissenschaften zu Göttingen, Mathematisch Physikalische Klasse 1918 (1918) 98–100.

[28] A.E. Danks, S.R. Hall, Z. Schnepp, The evolution of 'sol–gel' chemistry as a technique for materials synthesis, Mater. Horiz. 3 (2016) 91–112. https://doi.org/10.1039/C5MH00260E.

[29] L. Esterowitz, J. Noonan, J. Bahler, ENHANCEMENT IN A Ho^{3+}–Yb^{3+} QUANTUM COUNTER BY ENERGY TRANSFER, Appl. Phys. Lett. 10 (1967) 126–127. https://doi.org/10.1063/1.1754876.

[30] N.M. Sangeetha, F.C.J.M. van Veggel, Lanthanum Silicate and Lanthanum Zirconate Nanoparticles Co-Doped with Ho^{3+} and Yb^{3+}: Matrix-Dependent Red and Green Upconversion Emissions, J. Phys. Chem. C 113 (2009) 14702–14707. https://doi.org/10.1021/jp904516s.

[31] X. Chai, J. Li, X. Wang, Y. Li, X. Yao, Upconversion luminescence and temperature-sensing properties of Ho^{3+}/Yb^{3+}-codoped $ZnWO_4$ phosphors based on fluorescence intensity ratios, RSC Adv. 7 (2017) 40046–40052. https://doi.org/10.1039/c7ra05846b.

[32] X.X. Zhang, P. Hong, M. Bass, B.H.T. Chai, Ho^{3+} to Yb^{3+} back transfer and thermal quenching of upconversion green emission in fluoride crystals, Appl. Phys. Lett. 63 (1993) 2606–2608. https://doi.org/10.1063/1.110445.

[33] X. Wei, Y. Li, X. Cheng, Y. Chen, M. Yin, Strong dependence of upconversion luminescence on doping concentration in holmium and ytterbium co-doped Y_2O_3 phosphor, J. Rare Earths 29 (2011) 536–539. https://doi.org/10.1016/S1002-0721(10)60493-0.